A study of using nonnegative matrix factorization to detect solder-voids from radiographic images of solder

Motoaki Mouri*, Yoichi Kato‡ Hiroshi Yasukawa‡ and Ichi Takumi§
*Faculty of Business Administration, Aichi University, Aichi, Japan
Email: mouri@aichi-u.ac.jp
†Brain Science Institute, RIKEN, Saitama, Japan
‡Grad. School of Information Science and Technology, Aichi Prefectural University, Aichi, Japan
§Dept. of Computer Science and Engineering, Nagoya Institute of Technology, Aichi, Japan

***Abstract*—Accurate detection of voids in solder bumps on ball grid arrays (BGAs) is important for improving device quality. Radiographic imaging is commonly used to inspect BGA packages incorporate into LSI circuits. In the case of conventional method, imaging is normally done four times, and the images obtained are averaged to reduce noises. We have developed a nonnegative matrix factorization method for detecting solder-voids using only three radiographic images. Computer simulation demonstrated that it has the same level of accuracy as the conventional method.**

I. Introduction

Daily life has become highly dependent on electronic devices. Devices such as engine control units with LSI circuitry incorporating ball grid arrays (BGAs) [1], [2], [3] are susceptible to failure due to voids in the solder bump contacts in the BGAs. Guaranteeing solder integrity is thus indispensable for achieving high-quality electronic devices. This means that voids in the solder bumps must be accurately detected.

The defects in solder bumps can be classified as cracks [4], voids [5], foreign substances [6], disconnections, or short circuits (bridges) [7]. Cracks, voids, and foreign substances cannot be detected in an electrical continuity test. Moreover, BGA packages cannot be visually examined because the solder bumps are hidden beneath the base plate. Therefore, two-dimensional (2D) radiographic imaging is commonly used to inspect solder bumps. It can be used to detect cracks, voids, and foreign substances when LSI's back substrate is unpopulated. Example 2D radiographic images of solder bumps are shown in Fig. 1. The left circle shows a solder bump with a void at the center, and the right circle shows one without a void. The bottom graph shows luminance of central horizontal direction (pointed by a triangle) of the image. If a solder bump has a void, the luminance of its part increases.

The common alternative to radiographic imaging is computed tomography (CT) imaging, which produces high-definition low-noise images. Example CT images of solder bumps are shown in Fig. 2. The image in the left rectangle shows a solder bump with a void, and the image in the right rectangle shows one without a void. Although CT imaging clearly reveals defects in solder bumps, the equipment is very expensive, and the imaging is a lengthy process because each image is reconstructed from many images. The time required for 2D radiographic imaging is shorter because only a few images are needed.

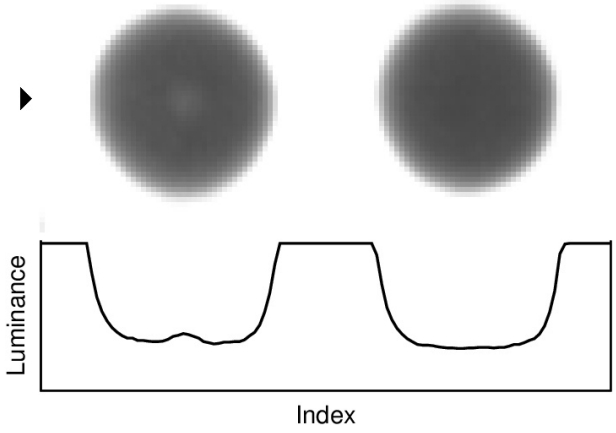

Fig. 1. 2D radiographic images of solder bumps with and without void

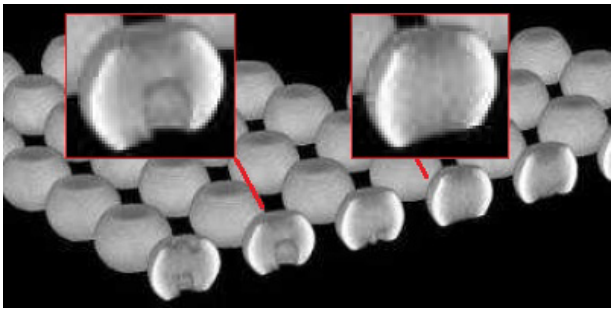

Fig. 2. CT images of solder bumps with and without void

Since 2D radiographic images are noisy compared to CT ones, image averaging is normally used to reduce the noise. A recently proposed noise reduction method uses discrete Fourier transformation and training data [8]. However, this method does not focus on the defect itself. To improve inspection accuracy, the defect must be detected. To reduce the processing time, the number of images used for averaging must be

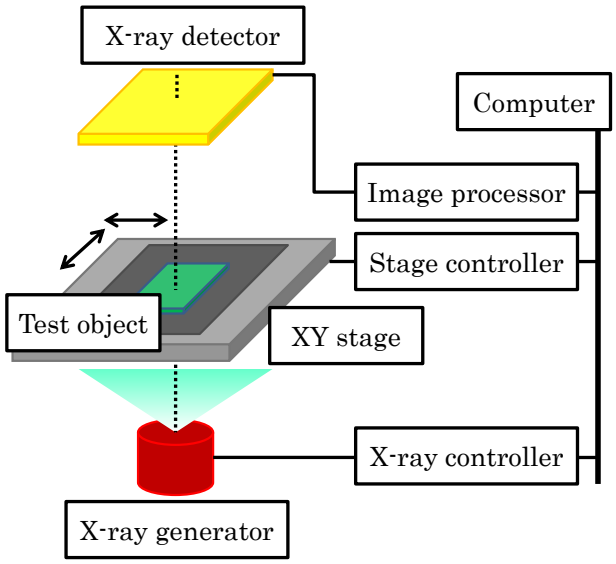

Fig. 3. Configuration of radiographic imaging equipment

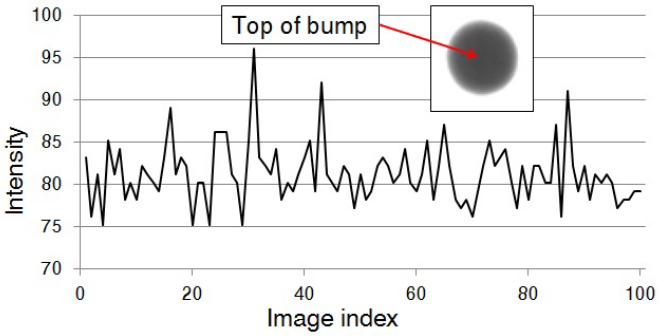

Fig. 4. Instability of X-ray generator

reduced.

We have developed a method for detecting solder-voids using only three 2D radiographic images. It estimates the height of the voids using nonnegative matrix factorization. Computer simulation demonstrated that it has the same level of accuracy as the four-image averaging method.

II. Radiographic Imaging

The configuration of the radiographic imaging equipment is shown in Fig. 3. An x-ray generator is placed directly beneath the BGA to be inspected, and an x-ray detector is placed above it. The distance between the generator and the detector is fixed in case of 2D radiographic imaging. Since the x-rays spread out as they move away from the point light source of the generator, the captured image of the BGA expands in accordance with the projection principle, enabling the 800 μm fine pitch structure of the BGA to be inspected.

Unfortunately, the output power of the x-ray generator is unstable, as shown in Fig. 4. The black circle in the figure shows an x-ray intensity image of a solder bump. The horizontal axis represents the image index, and the vertical axis represents the intensity at the top of this bump. The intensity

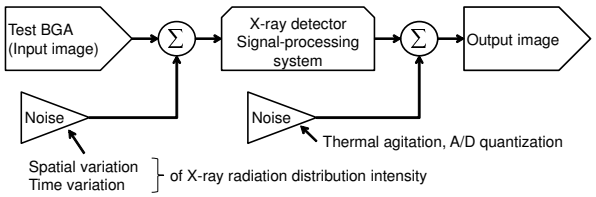

Fig. 5. Noise model assumed for radiographic imaging

changed even though the same solder bump was used. This is because only 1 % of the energy input into the generator was changed into x-rays; 99 % became waste heat. The common way of overcoming this problem is to average several images of the same bump.

The noise model assumed for radiographic imaging is shown in Fig. 5. The key noise factor is the spatiotemporal variation in the x-ray radiation distribution intensity although the x-ray detector and the signal-processing system sometimes generate slight noise. Not only is the output power unstable, but the sensor noise is also unstable.

III. Conventional Solder-Void Estimation Method

The height of a solder bump is represented by l, the sensor value x is given by

$$x = a \cdot \exp(-\mu l) \tag{1}$$

where a is the x-ray irradiation intensity, and μ is the attenuation coefficient, which depends on the type of material and the spectrum of the generated x-rays. We can presume the μ is static because the material and the spectrum did not change between imagings. If the solder bump has a void, we can replace (1) with

$$x = a \cdot \exp(\mu(v - l_0)) \tag{2}$$

where l_0 is the original height of the solder bump, and v is the height of the void.

To take into account the instability of the x-ray generator and sensor noise, we replace Equation (2) with

$$x = (a + \Delta a) \cdot \exp(\mu(v - l_0)) + \Delta x \tag{3}$$

where Δa is the difference from the set intensity, and Δx is sensor noise. We can then estimate v by using an inverse operation like

$$v = l_0 + \frac{1}{\mu} \cdot (\log(x - \Delta x) - \log(a + \Delta a)) \tag{4}$$

We want to reduce Δx and Δa in (4) to 0 as much as possible. The simplest technique for achieving that is averaging. When v is averaged using n radiographic images, the averaged v is given by

$$\begin{aligned} \bar{v} &= \frac{1}{n}\sum_{i=1}^{n} v_i \\ &= l_0 + \frac{1}{n\mu}\sum_{i=1}^{n}(\log(x - \Delta x_i) - \log(a + \Delta a_i)) \end{aligned} \tag{5}$$

where i is the image index. Hereafter, we call this technique order pattern "OP1." If n is not so large, using (5) may not reduce the noise enough because of nonlinearity. We thus need to reduce the noise more steadily in order to reduce the number of imagings from four to three.

The average x when n radiographic images are averaged is given by

$$\begin{aligned}\bar{x} &= \frac{1}{n}\sum_{i=1}^{n} x_i \\ &= \left(a + \frac{1}{n}\sum_{i=1}^{n}\Delta a_i\right)\cdot\exp\left(\mu\left(v - l_0\right)\right) + \frac{1}{n}\sum_{i=1}^{n}\Delta x_i \quad (6)\end{aligned}$$

If we assume that the expected values of Δx and Δa close to 0, the errors become small due to the central limit theorem, as given by using standerd deviations σ_x and σ_a like

$$\hat{v} = l_0 + \frac{1}{\mu}\cdot\left(\log\left(x - \frac{\sigma_x}{\sqrt{n}}\right) - \log\left(a + \frac{\sigma_a}{\sqrt{n}}\right)\right) \quad (7)$$

Hereafter, we call this technique order pattern "OP2."

IV. Solder-void detection using NMF

A. Nonnegative matrix factorization

Nonnegative matrix factorization (NMF) [9] is one way to approximately factorize a given nonnegative matrix under nonnegativity constraints. The $n \times T$ matrix $\boldsymbol{X} = [\boldsymbol{x}(1), \boldsymbol{x}(2), ..., \boldsymbol{x}(T)]$, which has only nonnegative values, is approximated by NMF as

$$\boldsymbol{X} \approx \boldsymbol{AY} \qquad \boldsymbol{X}, \boldsymbol{A}, \boldsymbol{Y} \geq 0 \quad (8)$$

where $\boldsymbol{A}$ is an $n \times r$ mixing matrix and $\boldsymbol{Y} = [\boldsymbol{y}(1), \boldsymbol{y}(2), ..., \boldsymbol{y}(T)]$ is an $r \times T$ component matrix. Both $\boldsymbol{A}$ and $\boldsymbol{Y}$ have only nonnegative values. The rank of factorization, r, is chosen as $nT > nr + rT$.

Equation (8) can be written column by column as $\boldsymbol{x}(t) \approx \boldsymbol{A}\boldsymbol{y}(t)$, where $\boldsymbol{x}(t)$ and $\boldsymbol{y}(t)$ correspond to the tth columns in $\boldsymbol{X}$ and $\boldsymbol{Y}$. This NMF model (Fig. 6) is an approximation of the linear mixture signal model. Setting rank r is important for accurate estimation.

NMF finds $\boldsymbol{A}$ and $\boldsymbol{Y}$ by using iterative updates on the basis of a cost function. Various NMF algorithms have been developed [10]. The one used here is the image space reconstruction algorithm (ISRA) [11], [12]. The cost function of the ISRA is the square of the Euclidean distance between $\boldsymbol{X}$ and $\boldsymbol{AY}$,

$$||\boldsymbol{X} - \boldsymbol{AY}||^2 = \sum_{ik}\{X_{ik} - [\boldsymbol{AY}]_{ik}\}^2 \quad (9)$$

This cost function is lower-bounded by zero and clearly vanishes if and only if $\boldsymbol{X} = \boldsymbol{AY}$. To minimize the cost function given by (9), the ISRA updates $\boldsymbol{A}$ and $\boldsymbol{Y}$ a sufficient number of times:

$$\begin{aligned}&A_{ij} \leftarrow A_{ij}\frac{[\boldsymbol{X}\boldsymbol{Y}^T]_{ij}}{[\boldsymbol{A}\boldsymbol{Y}\boldsymbol{Y}^T]_{ij}}, \quad Y_{jk} \leftarrow Y_{jk}\frac{[\boldsymbol{A}^T\boldsymbol{X}]_{jk}}{[\boldsymbol{A}^T\boldsymbol{A}\boldsymbol{Y}]_{jk}} \\ &A_{ij} \leftarrow \frac{A_{ij}}{\sum_j A_{ij}} \quad (10)\end{aligned}$$

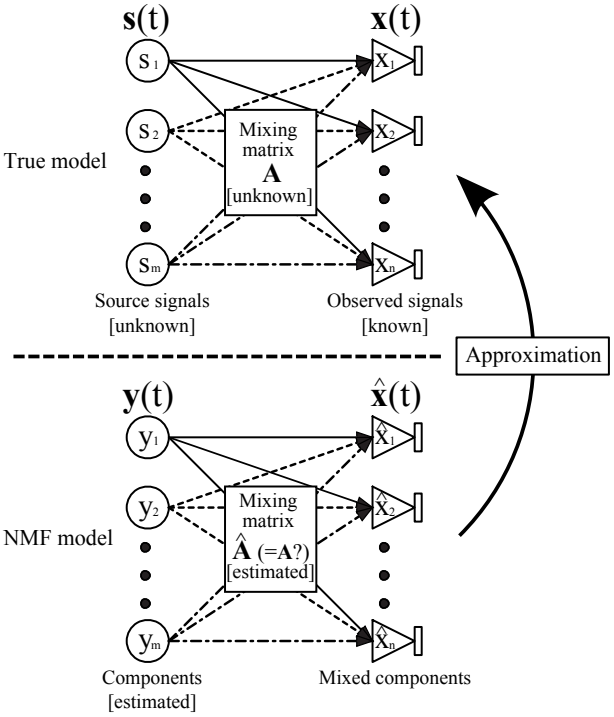

Fig. 6. NMF model

B. Void estimation using NMF

We can apply NMF to our problem because the pixel values for radiographic images are nonnegative. The ist 2D map image is converted into raw vector $X_i(t),\ (t = 1, 2, ..., T)$, and input matrix $\boldsymbol{X}$ is composed of these vectors.

Generally, NMF is based on the assumption of several source components. Here, the source components are ideally the original height of solder bump l_0 and the height of the void v. However, NMF cannot separate components because the component ratios are the same in the input radiographic images X_i. The differences are only the scalability of intensity and sensor noise. To overcome this problem, we replace the 4th input image X_4 with the standard radiographic image x_{ref} as a reference. Ideally, x_{ref} is defined as $x_{\mathrm{ref}} = x_0 = \exp(-\mu l_0)$.

If NMF works properly, Δx in (3) is removed because it is included in the approximation error of $\boldsymbol{X} - \hat{\boldsymbol{A}}\boldsymbol{Y}$. The scalability of intensity $a + \Delta a_i$ is estimated as the elements in $\hat{\boldsymbol{A}}$. However, the source components l_0 and v cannot be estimated directly. So, if we estimate $(a + \Delta a_i)\cdot x_0$ as $\hat{A}_{i1}Y_1$, we can estimate v_i using

$$\begin{aligned}\hat{v}_i &= -\frac{1}{\mu}\cdot\left(\log\left(\hat{A}_{i1}Y_1\right) - \log\left(\hat{\boldsymbol{A}}_i\boldsymbol{Y}\right)\right) \\ &= -\frac{1}{\mu}\cdot\left(\log\left((a + \Delta a_i)\cdot x_0\right)\right. \\ &\qquad \left. - \log\left((a + \Delta a_i)\cdot\exp\left(l_0 - v\right)\right)\right) \\ &= -\frac{1}{\mu}\cdot\left(\log\left(\exp\left(-\mu l_0\right)\right) - \log\left(\exp\left(\mu(l_0 - v)\right)\right)\right) \\ &= l_0 - (l_0 - v) = v \quad (11)\end{aligned}$$

NMF does not provide a unique solution. The results are affected by the initial matrices. This means that good initial

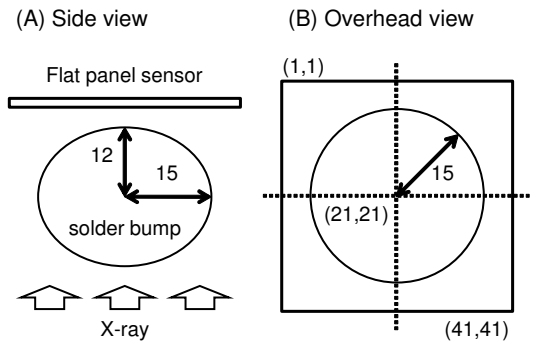

Fig. 7. Configuration of ideal solder bump

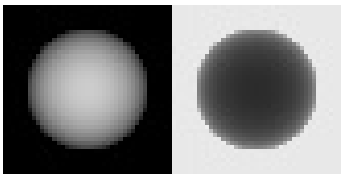

Fig. 8. Images of ideal solder bump: (left) l_0, (right) x_0

matrices are needed to obtain the desired results. We set Y_1 and Y_2, the 1st and 2nd raw values of initial component matrix $\boldsymbol{Y}$, to

$$\boldsymbol{Y} = \begin{pmatrix} Y_1 \\ Y_2 \end{pmatrix} = \begin{pmatrix} 4 \cdot x_{\mathrm{ref}} \\ \sum_{i=1}^{3} X_i - 3 \cdot x_{\mathrm{ref}} \end{pmatrix} \tag{12}$$

We set initial mixing matrix $\hat{\boldsymbol{A}}$ to

$$\hat{\boldsymbol{A}} = \begin{pmatrix} 1/4 & 1/3 \\ 1/4 & 1/3 \\ 1/4 & 1/3 \\ 1/4 & 0 \end{pmatrix} \tag{13}$$

Since X_4 is reference input, it is best to fix the values $\hat{A}_{41}$, $\hat{A}_{42}$, and Y_1. Therefore, we do not update $\hat{A}_{41}$, $\hat{A}_{42}$, and Y_1 in each iteration. Hereafter, we call the NMF algorithm using this fixing technique "NMF_fixed."

V. Computer simulation

A. Conditions

A solder bump is an oblate spheroid; i.e., it is slightly flattened at the poles. Therefore, we configured the ideal solder bump as shown in Fig. 7. The map size of a radiographic image for a solder bump is 41×41, and the central index of the image is $(21, 21)$. Left and right radiographic images of an ideal solder bump are shown in Fig. 8.

For this computer simulation, we generated 400 data set of solder bumps with one void each and 100 data set of bumps without voids (Fig. 9). We assumed that the voids had a spherical shape and set the radii of the voids from 1.00 to 5.75. The position coordinates of each void were set randomly within the solder bump. The void radius and position were the same for all the bumps in each data set. Attenuation coefficient μ was set to a fixed value of 0.07.

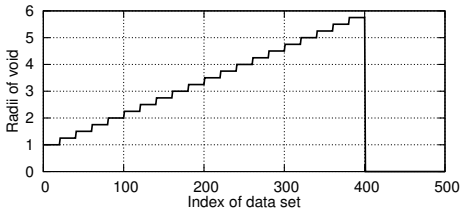

Fig. 9. Radii of voids corresponding to each data set

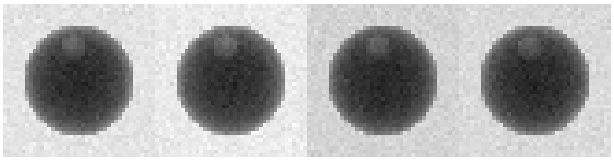

Fig. 10. Generated radiographic images (void radius of 3.5)

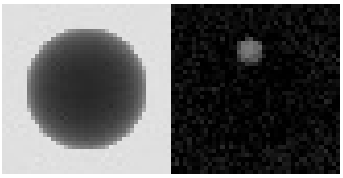

Fig. 11. Source components estimated by NMF: (left) Y_1, (right) Y_2

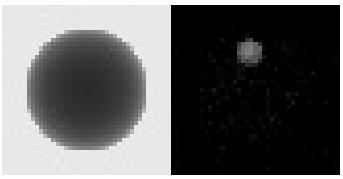

Fig. 12. Source components estimated by NMF_fixed: (left) Y_1, (right) Y_2

We obtained four images for each data set. Their x-ray intensities were randomly set from 0.85 to 1.15. The distribution of the sensor noise was assumed to be Gaussian, with a mean of 0 and a standard deviation of 0.0244 (3% of difference between minimum and maximum values for ideal solder bump). The intensity and noise were set for each image.

B. Results

An example of four radiographic images generated for one bump is shown in Fig. 10. The gray circle at the top of the black circle is a void with a radius of 3.5. The images are noisy and have different intensities. We detected the void from these images.

Figure 11 shows images of the source components estimated using NMF. The left one indicates Y_1, and the right one indicates Y_2. Note that we used only the first three images in Fig. 10. We can consider Y_1 as an image of the ideal solder bump, and we can consider Y_2 as the effect of the void. However, Y_2 has some noise. Figure 12 shows the images of source components estimated using NMF_fixed. Compared to Fig. 11, the errors in Y_2 were lower, indicating that our fixing technique suppressed the effect of noise in Y_2.

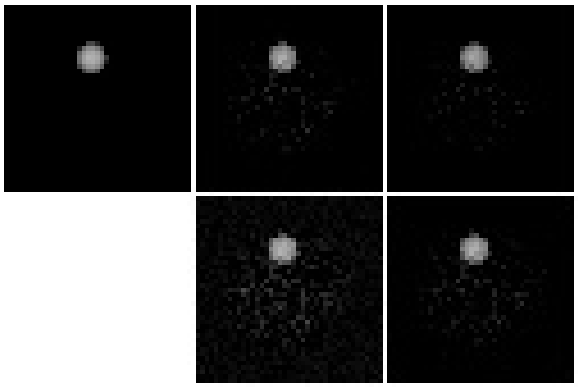

Fig. 13. Estimated height of voids (OP1); (upper left) ideal, (upper middle) three-image average, (upper right) four-image average, (lower middle) NMF, (lower right) NMF_fixed

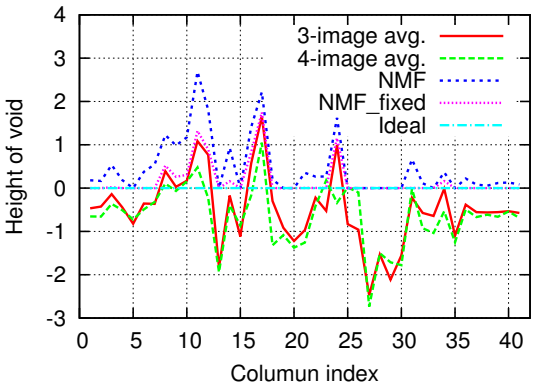

Fig. 14. Estimated height of voids in 21th row (OP1)

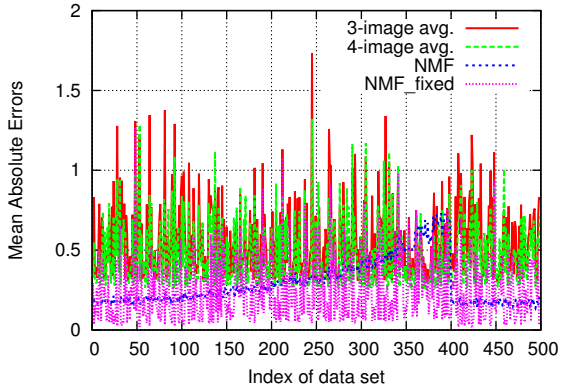

Fig. 15. Mean absolute errors for estimated voids (OP1)

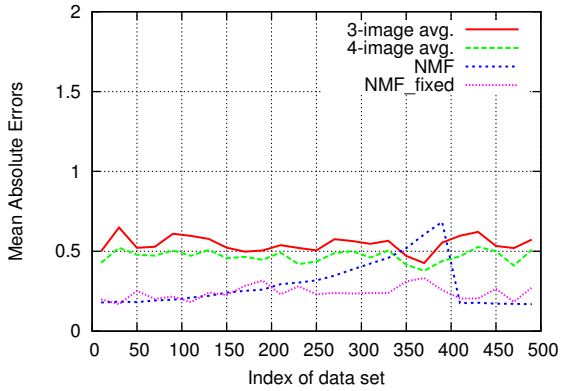

Fig. 16. Mean absolute errors for estimated voids (OP1)

Figure 13 shows the height of the void imaged in Fig. 10 as estimated using each method for the inverse-operation $\rightarrow$ averaging order pattern (OP1). The upper left image shows the ideal height, the upper middle (right) image shows the result of averaging 3 (4) images, and the lower middle (right) figure shows the result of using NMF (NMF_fixed). Although simple averaging appears to have well estimated the void, there were many negative values. An example is shown in Fig. 14. On the other hand, there are no negative values in the height of voids estimated by using NMF or NMF_fixed. The maximum value was 6.76 using three images and 6.47 using four images although the ideal height was between 0 and 3.5. In contrast, the results with NMF_fixed did not have negative values, and the maximum value was 5.45. The mean absolute error was reduced from 0.58 (three images) and from 0.65 (four images) to 0.06.

The numerical evaluation results for each data set for OP1 are plotted in Fig. 15. The vertical axis represents the mean absolute error, and the horizontal axis represents the data set index. The void radius increased with the index (0.25 for each 20 data sets from 1.0 to 5.75). The data sets from 401 to 500 did not have voids. This graph indicates that the results with NMF_fixed were more accurate than those with simple averaging.

Figure 16 shows the mean absolute errors. They were averaged for each 20 data sets (for which the void radii were the same). The error for NMF increased with the index, i.e., the void radius, while that for NMF_fixed remained small. These results show that our method works as well as the four-image averaging method although only three images are used for the averaging.

Figure 17 shows the height of the void imaged in Fig. 10 as estimated using each method for the averaging $\rightarrow$ inverse-operation order pattern (OP2). The errors were slightly less than those shown in Fig. 13. However, it seems that the height of voids estimated by NMF or NMF_fixed have bias in Fig. 18. The numerical evaluation results are shown in Figs. 19 and 20. They were almost the same even though we changed the order of applied techniques.

VI. Conclusions

The method we developed for detecting solder-voids uses nonnegative matrix factorization and radiographic imaging. Computer simulation demonstrated that our method works as well as simple averaging although only three images (rather than four) are used for averaging. However, the error increased with the void radius. The results were basically the same when the techniques were applied in a different order.

Future work includes applying our method to actual data and evaluating the results. It also includes developing a de-

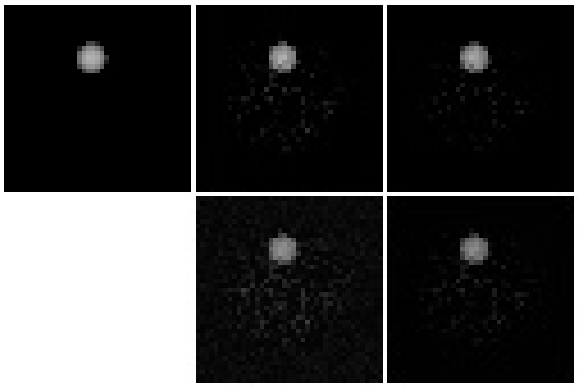

Fig. 17. Estimated height of voids (OP2); (upper left) ideal, (upper middle) three-image average, (upper right) four-image average, (lower middle) NMF, (lower right) NMF_fixed

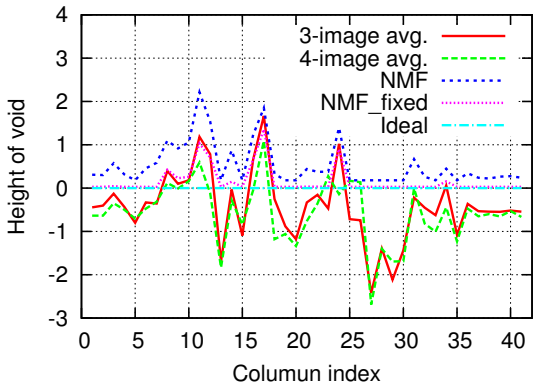

Fig. 18. Estimated height of voids in 21th row (OP2)

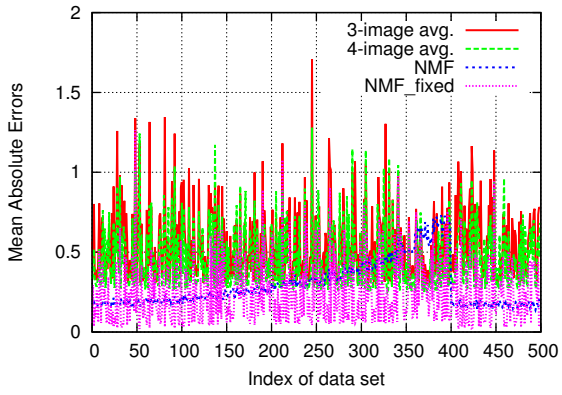

Fig. 19. Mean absolute errors for estimated voids (OP2)

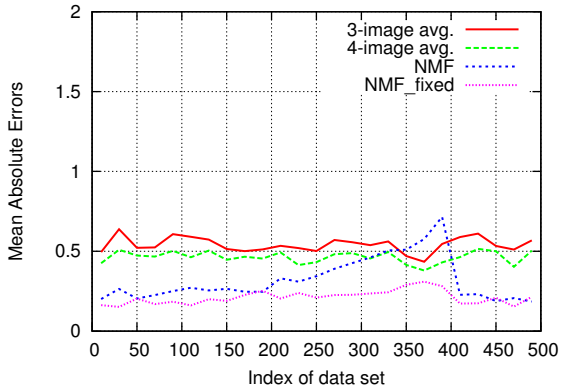

Fig. 20. Mean absolute errors for estimated voids (OP2)

fect inspection method that uses the results provided by our proposed method.

ACKNOWLEDGMENT

This research has been supported by Nagoya Electric Works Co., Ltd., which provided the 2D radiographic imaging equipment and several of the images shown. We are grateful to Dr. Andrzej Cichocki of the Riken Brain Science Institute for providing the source code on which our NMF program is based.

REFERENCES

[1] Y. Sato, S. Tanaka, S. Yoshida, S. Ohtsuji, T. Hotta, H. Tanaka: System Control LSI Reflecting Data Directly on Main Memory for Highly Reliable Controller, in Japanese, *TECHNICAL REPORT OF IEICE. ICD*, Vol. 98, No. 23, pp. 101-108, 1998.

[2] Y. Shimada: 3 Dimentional Memory Module Using CSP (¡Special Article¿Trend of BGA · CSP · KGD), in Japanese, *Journal of Japanese Institute of Electronics Packaging*, Vol. 1, No. 5, pp. 371-375, 1998.

[3] H. Yamaguchi, A. Teramoto, T. Iri, I. Horiba, N. Sugie: Extracting Solder Joints of CSP from X-ray Images, in Japanese, *TECHNICAL REPORT OF IEICE. ICD*, Vol. 98, No. 335, pp. 371-375, 1998.

[4] R. Nakahara, N. Yoshida N. Tada: 1511 Effect of Copper Wire Location and Voids on Evaluation of Interface Crack between Solder Ball and Copper by Direct Current Potential Difference Method, in Japanese, *Computational Mechanics Division Conference Lecture collected papers*, Vol. 2009, No. 22, pp. 724-725, 2009.

[5] T. Terasaki, H. Tanie, K. Kojima: 1850 Effect of Displacement Amplitude on Fatigue Crack Paths for Ball Grid Array Solder Joints including Void, in Japanese, *JSME annual meeting*, Vol. 2005, No. 6, pp. 277-278, 2005.

[6] K. Noguchi, A. Teramoto, M. Yamada, T. Murakoshi: Inspection Technique of Foreign Objects in BGA Solder Joint Using Oblique X-ray Computed Tomography, in Japanese, *Journal of Japanese Institute of Electronics Packaging*, Vol. 13, No. 1, pp. 63-70, 2010.

[7] T. Hamada, K. Nakahata, S. Fushimi, Y. Morioka, T. Nishida: Automatic Solder Joint Inspection System by X-ray Imaging, in Japanese, *JSPE*, Vol. 59, No. 1, pp. 65-71, 1993.

[8] Y. Kato, T. Tanizaki, H. Yasukawa: A study on test image production using frequency domain correlation with convex function for radiographic inspection equipments, *The 22nd IEEE International Symposium on Industrial Electronics Proceeding*, 2013.

[9] A. Cichocki, R. Zdunek, A.-H. Phan and S. Amari: *Nonnegative Matrix and Tensor Factorizations: Applications to Exploratory Multi-way Data Analysis and Blind Source Separation*, Chichester: Wiley, 2009.

[10] A. Cichocki, R. Zdunek, *NMFLAB toolboxes* [http://www.bsp.brain.riken.jp/ICALAB/nmflab.html], 2009.

[11] M. E. Daube-Witherspoon and G. Muehllehner: An iterative image space reconstruction algorithm suitable for volume ECT, *IEEE Trans. Med. Imaging*, vol. MI-5, No. 2, pp. 61-66, 1986.

[12] D. D. Lee and H. S. Seung: Learning the parts of objects by nonnegative matrix factorization, *Nature*, vol. 401, pp. 788-791, 1999.